Article

Disruption of seasonal influenza circulation and evolution during the 2009 H1N1 and COVID-19 pandemics in Southeastern Asia

Zhiyuan Chen[1], Joseph L.-H. Tsui [2,3], Jun Cai [1], Shuo Su[1,4], Cécile Viboud [5], Louis du Plessis [6,7,10], Philippe Lemey [8,10] ✉, Moritz U. G. Kraemer [2,3,10] ✉ & Hongjie Yu [1,4,9,10] ✉

East, South, and Southeast Asia (together referred to as Southeastern Asia hereafter) have been recognized as critical areas fuelling the global circulation of seasonal influenza. However, the seasonal influenza migration network within Southeastern Asia remains unclear, including how pandemic-related disruptions altered this network. We leveraged genetic, epidemiological, and airline travel data between 2007-2023 to characterise the dispersal patterns of influenza A/H3N2 and B/Victoria viruses both out of and within Southeastern Asia, including during perturbations by the 2009 A/H1N1 and COVID-19 pandemics. During the COVID-19 pandemic, consistent autumn-winter movement waves from Southeastern Asia to temperate regions were interrupted for both subtype/lineages, however the A/H1N1 pandemic only disrupted A/H3N2 spread. We find a higher persistence of A/H3N2 than B/Victoria circulation in Southeastern Asia and identify distinct pandemic-related disruptions in A/H3N2 antigenic evolution between two pandemics, compared to interpandemic levels; similar patterns are observed in B/Victoria using genetic distance. The internal movement structure within Southeastern Asia markedly diverged during the COVID-19 pandemic season, and to a lesser extent, during the 2009 A/H1N1 pandemic season. Our findings provide insights into the heterogeneous impact of two distinct pandemic-related disruptions on influenza circulation, which can help anticipate the effects of future pandemics and potential mitigation strategies on influenza dynamics.

Seasonal influenza infections occur annually and cause a significant disease burden across the world[1]. Human mobility and interconnectedness is thought to be the main driver of worldwide human influenza virus spread[2], while a combination of antigenic evolution to escape immunity and waning immunity results in an oscillating supply of susceptible hosts leading to frequent reinfections[3]. Seasonal influenza viruses cause predictable annual epidemics in temperate regions as well as relatively divergent waves in tropical regions[4,5]. Newly-emerged influenza viruses can disrupt this pattern through cross-subtype population immunity[6,7]. In parallel, other co-circulating

[1]School of Public Health, Key Laboratory of Public Health Safety, Ministry of Education, Fudan University, Shanghai, China. [2]Department of Biology, University of Oxford, Oxford, UK. [3]Pandemic Sciences Institute, University of Oxford, Oxford, UK. [4]Shanghai Institute of Infectious Disease and Biosecurity, Fudan University, Shanghai, China. [5]Fogarty International Center, National Institutes of Health, Bethesda, MD, USA. [6]Department of Biosystems Science and Engineering, ETH Zürich, Basel, Switzerland. [7]Swiss Institute of Bioinformatics, Lausanne, Switzerland. [8]Department of Microbiology, Immunology and Transplantation, Rega Institute, KU Leuven, Leuven, Belgium. [9]Department of Infectious Diseases, Huashan Hospital, Fudan University, Shanghai, China. [10]These authors jointly supervised this work: Louis du Plessis, Philippe Lemey, Moritz U. G. Kraemer, Hongjie Yu ✉e-mail: philippe.lemey@kuleuven.be; moritz.kraemer@biology.ox.ac.uk; yhj@fudan.edu.cn

seasonal or novel respiratory pathogens can shape the spread of seasonal influenza viruses, especially when they are associated with human behavioural changes in response to non-pharmaceutical interventions (NPIs) and declarations of public health emergencies[8,9]. Two emerging pathogens, the swine-origin influenza A/H1N1 virus and SARS-CoV-2, triggered global pandemics in 2009 and 2020 respectively. However, whether and how changes in human behaviour and cross-subtype population immunity during the course of these pandemics affected seasonal influenza circulation, especially in Southeastern Asia (here defined as East, South, and Southeast Asia), remains unclear.

Our previous work evaluated the global dispersal patterns of four seasonal influenza subtypes/lineages (A/H3N2, A/H1N1pdm09, B/Victoria and B/Yamagata) among 12 broad geographical regions prior, during, and after the COVID-19 pandemic, and found that the pandemic's onset led to a shift in the intensity and structure of the international movement of influenza lineages[10]. Beyond the global perspective focusing only on the COVID-19 or A/H1N1 pandemics alone[7,8,10], comparisons of the impacts of the 2009 A/H1N1 and COVID-19 pandemics on influenza circulation at a finer spatial scale are still lacking. Apart from the heterogeneity in the intensity of NPIs during the two pandemics, different degrees of viral interference (namely, virus–virus interactions via cross-immunity) can also be expected between seasonal influenza viruses and the two pandemic viruses[6,11,12]. Additionally, the structure of the influenza virus migration network within Asia, especially Southeastern Asia, has rarely been explored. Understanding the internal migration network within Southeastern Asia is critical as it has been suggested to play an essential role in generating antigenically distinct seasonal viruses and seeding global seasonal influenza epidemics[4,13,14]. Changes in human behaviour and cross-immunity during the 2009 A/H1N1 and COVID-19 pandemics provide natural experiments to evaluate temporal shifts on the circulation patterns of seasonal influenza in Southeastern Asia relative to the baseline interpandemic period, and elucidate the mechanisms at play. A comprehensive genomic and epidemiological assessment of the interplay between pandemic-related disruptions and seasonal influenza circulation in Southeastern Asia can further inform potential strategies for mitigating global disease burdens in the future.

In this study, we leveraged genetic, epidemiological, and airline travel data to assess the circulation dynamics of seasonal influenza emanating from and within Southeastern Asia between 2007 and 2023, covering the apexes of two global pandemics and multiple interpandemic seasons. Specifically, we first inferred the seasonality of viral movement out of Southeastern Asia, and identified those viral lineages that potentially persisted within Southeastern Asia (defined as persistent lineages) to trace their internal circulation dynamics. We subsequently performed long-term comparisons of the internal spread of seasonal influenza within Southeastern Asia and evaluated how influenza circulation was impacted by the two pandemics.

Results

Disruptions of influenza A/H3N2 and B/Victoria activity during pandemic seasons

To synchronise with the northern hemisphere influenza seasons (from July 1st of one year to June 30th of the next year[15,16]), the 2009 A/H1N1 and COVID-19 pandemic periods were respectively defined as spanning from July 2009 to June 2010 and from July 2020 to June 2021, with the periods between them labelled as the interpandemic periods/seasons. Similar to our previous work relating specifically to the COVID-19 pandemic period[10], the sampling intensity of virological surveillance for seasonal influenza during the two pandemic seasons was no lower than during previous seasons (Fig. 1a). The amplitude of surveillance intensity fluctuated across region and time, with a large increase directly after the start of the A/H1N1 pandemic and a generally increasing trend thereafter (Fig. 1a). Yearly fluctuations in viral

sampling were observed in temperate regions, peaking in their respective winter months (Fig. 1a, b). On the other hand, surveillance intensity within any given year remained relatively stable in Southeastern Asia (Fig. 1a, b), due to persistent influenza circulation throughout the year in large parts of the region[17,18].

Given the emergence of A/H1N1pdm09 in 2009[19] and the subsequent replacement of the previously circulating seasonal A/H1N1 virus, as well as the potential elimination of B/Yamagata in 2020[20], we focused on the remaining two human influenza subtypes/lineages, A/H3N2 and B/Victoria, for which we could study disruptions associated with two pandemic seasons. Initially, we established the average curve of positivity rate (as a proxy of influenza activity[21]) for seasons in the interpandemic period following epidemic alignment by peak week (details in "Methods", Supplementary Figs. 1, 2) as a baseline, against which the positivity rates during the two pandemic seasons were contextualised (Fig. 1c–e, g–i).

In temperate regions we observe a single annual winter wave of A/H3N2 circulation during the interpandemic period, while biannual peaks are observed in Southeastern Asia. Compared to interpandemic averages, extremely low A/H3N2 positivity rates were observed in all three regions throughout the two pandemics, except for a single peak occurring in Southeastern Asia in late August 2009 during the A/H1N1 pandemic, without a subsequent second peak (Fig. 1c–e). This single A/H3N2 wave was hypothesised to be associated with limited implementation of NPIs during the A/H1N1 pandemic[22], while the absence of a second peak could be attributable to viral interference due to large-scale transmission of the novel A/H1N1 pandemic virus[23], presumably via heterosubtypic cross-immunity[6]. The low positivity rate of A/H3N2 during the COVID-19 pandemic in all regions further highlights the impact of human behavioural changes on influenza circulation.

Despite variations in B/Victoria activity from season to season, we observe a single peak in all three regions during the interpandemic period, with a lower and usually delayed peak compared to A/H3N2 (Fig. 1g–i). A larger than usual wave of B/Victoria occurred in Southeastern Asia in January–March 2010 during the A/H1N1 pandemic, whereas little circulation was observed during the COVID-19 pandemic (Fig. 1i). In Southeastern Asia, the decline of B/Victoria positivity in 2020 was strongly associated with the reduction of among-country airline traffic flow (Pearson correlation coefficient: 0.89), after controlling for seasonality (calculating the changes relative to the baseline month before the pandemic).

The two pandemics occurred under heterogeneous conditions (Supplementary Table 1, Supplementary Figs. 3–5). Since there are few records of the stringency of travel measures and NPIs during the H1N1 pandemic, we calculated an air travel-related stringency index (other behavioural changes are not included), based on the strong correlation between airline traffic and the COVID-19 stringency index during the COVID-19 pandemic (Supplementary Table 2). In comparison to the 2009 H1N1 pandemic, the COVID-19 pandemic was associated with a far higher air travel-related stringency index (Supplementary Fig. 3). To further determine correlates with seasonal influenza activity during the pandemic seasons, we built a random forest model to assess the importance of predictors. We identified the COVID-19 stringency index as the most important predictor associated with the decline of seasonal influenza activity during the COVID-19 pandemic, while the socio-demographic index (a composite indicator constructed from income per capita, average years of schooling, and total fertility rate[24]) played the most important role during the 2009 A/H1N1 pandemic (Supplementary Fig. 6).

Influenza A/H3N2 and B/Victoria movements from Southeastern Asia to temperate regions

Given the heterogeneous spatiotemporal distribution of genetic sequences (Fig. 1f, j), we adopted three sub-sampling schemes to select sequences and assess the potential impact of sampling biases
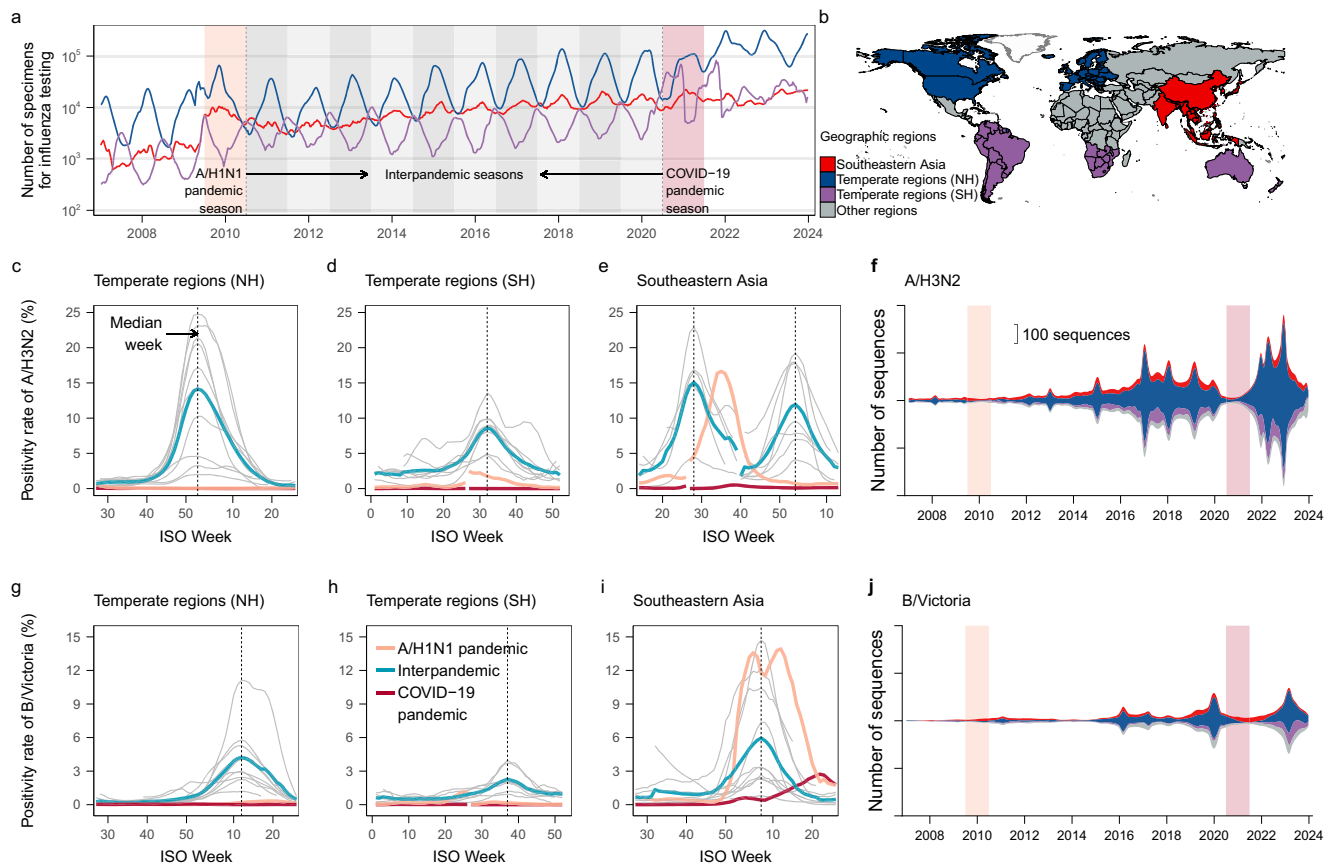
Fig. 1 | Variation in testing intensity, positivity rate, and numbers of HA gene sequences of seasonal influenza viruses in Southeastern Asia and temperate regions of the northern hemisphere (NH) and southern hemisphere (SH). a A five-week running average of the number of specimens tested for influenza in three geographic regions. Light and dark red shading denote the A/H1N1 and COVID-19 pandemic seasons, respectively, between which are interpandemic seasons. Global-scale data after 2017, presented in Fig. 1a of our previous study[10], have been re-aggregated into three regions and are retained here for the comparisons between the two pandemic seasons. **b** Geographic divisions used in this study. The entirety of South America was grouped with the Southern Hemisphere given recommended use of the Southern Hemisphere vaccine formulation throughout the region[5,54]. **c–e** Average positivity rates for A/H3N2 for seasons in the interpandemic period (cyan-blue lines) versus that during the 2009 A/H1N1 pandemic season (orange lines) and the COVID-19 pandemic season (red lines). Cyan-blue lines represent mean positivity rates for A/H3N2 after aligning the median week of peak (shown as

the dashed line) for the seasons in the interpandemic periods, where grey lines show the five-week rolling positivity rate for each season separately after epidemic alignment. The processing details have been presented in Supplementary Figs. 1, 2. ISO week 53 was removed for some years to maintain temporal consistency. Two epidemic alignments of A/H3N2 were performed in Southeastern Asia by splitting each influenza season into a summer (corresponding to the summer peak) and winter season (corresponding to the winter peak). In (**d**, **h**) the first half of the positivity lines (Jan–Jun 2010; Jan–Jun 2021) during the pandemic periods occurred after the second half of the line (Jul–Dec 2009; Jul–Dec 2020), for temporal comparison. In (**e**) the first half of the positivity lines (Apr–Jun 2010; Apr–Jun 2021) during the pandemic periods occurred after the second half of the lines (Jul 2009–Mar 2010; Jul 2020–Mar 2021). **f** HA gene sequences of A/H3N2 stratified by geographic regions over time. **g–i** Same as (**c–e**) but for B/Victoria. **j** Same as (**f**) but for B/Victoria.

(Supplementary Fig. 7). We first extended a previous study[10] by performing a two-state discrete trait analysis to estimate Markov jump events (referred to as viral movement events) between Southeastern Asia and temperate regions from 2007 to 2023 (Supplementary Fig. 8 and Fig. 2). All three sub-sampling schemes resulted in similar numbers of viral movements between locations over time, for both subtypes/lineages (Supplementary Fig. 8), indicating that the signal is robust to the sub-sampling scheme. In our main analysis we employed an even sub-sampling scheme by time and location (details in "Methods"), as it has been shown to be more robust to sampling bias[25]. Despite selecting a similar number of genetic sequences from both regions, a higher frequency of A/H3N2 movements from Southeastern Asia to temperate regions was detected, compared to the reverse direction (Fig. 2a). Regarding B/Victoria lineages, the pattern of bidirectional movements between the two regions varied widely from season to season (Supplementary Fig. 8d–f), but with a more balanced flux than A/H3N2 (Fig. 2a, b).

After aligning the peaks of each season to their median epidemic week, we subsequently averaged the number of viral movement events

from Southeastern Asia to temperate regions during the interpandemic period. As a baseline, A/H3N2 movement from Southeastern Asia gradually peaked in early December in interpandemic seasons (Fig. 2c), while B/Victoria movements peaked in January, although with a heavy tail toward earlier weeks, indicating sustained movements starting much earlier (Fig. 2d). During the two pandemics, the typical A/H3N2 winter peak in exports from Southeastern Asia disappeared. During the A/H1N1 pandemic, B/Victoria movement peaked at the same time as during the interpandemic period, and at a level consistent with interpandemic activity. This coincides with the large B/Victoria wave in Southeastern Asia during the same time period, indicating sustained exports from Southeastern Asia, but not establishment in temperate regions (Fig. 1g–i). However, no corresponding B/Victoria winter peak was detected during the COVID-19 pandemic.

Persistent influenza lineages within Southeastern Asia

To enable further reconstruction of the internal network within Southeastern Asia, we categorised the viruses circulating in Southeastern Asia based on whether they had been inferred to have either
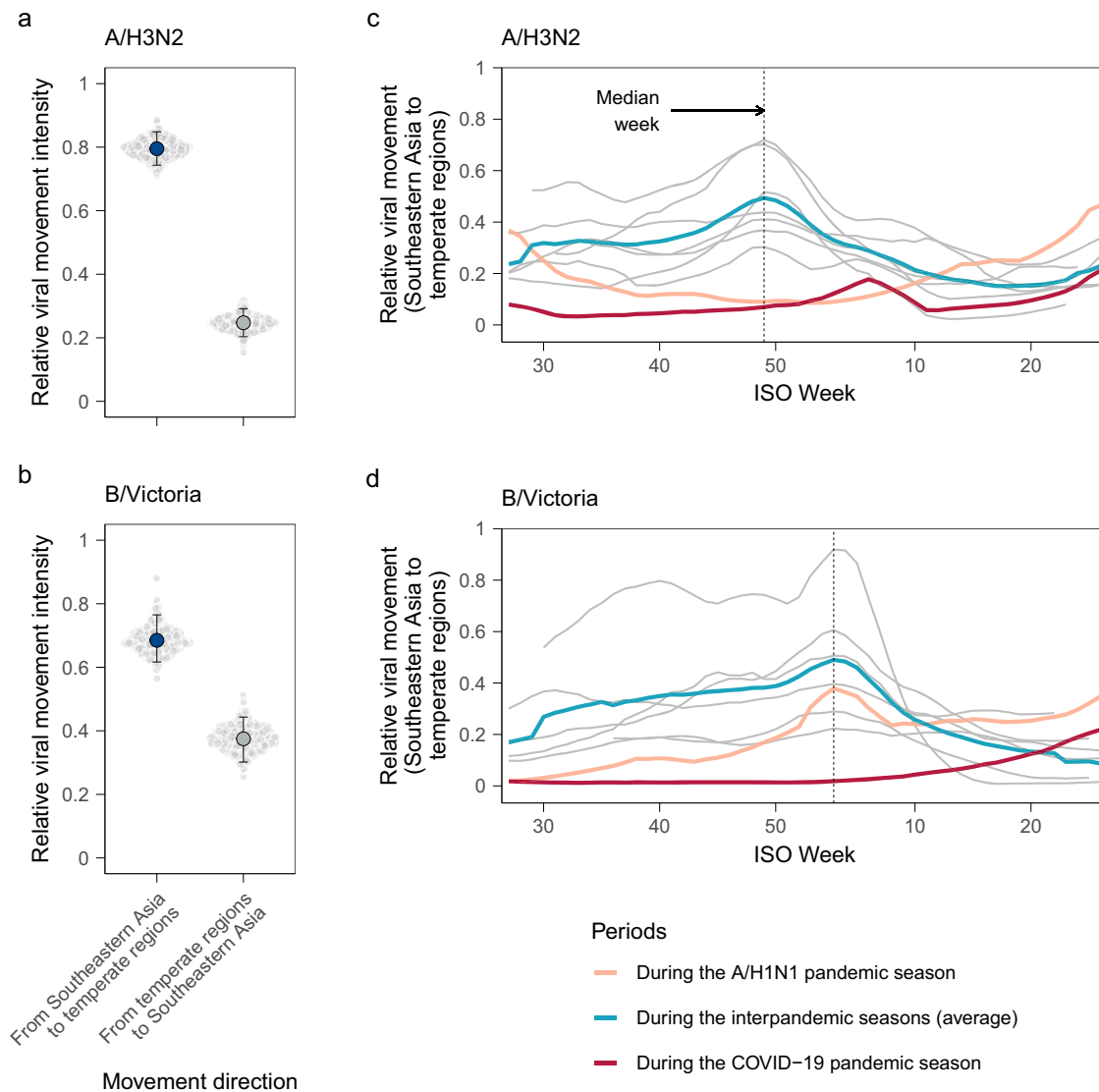
Fig. 2 | Inferred movement of A/H3N2 and B/Victoria between Southeastern Asia and temperate regions under the even sub-sampling scheme. a–b The overall relative viral movement intensity in each direction over the entire time period of interest (A/H1N1 pandemic season, interpandemic seasons, and COVID-19 pandemic season). Posterior mean estimates (blue points) with 95% HPD intervals (error bars) are shown, based on $n = 901$ (**a**) and $n = 514$ (**b**) post-burnin samples. The scale of relative values is comparable between (**a**) and (**b**). **c–d** Average relative viral movement intensity of A/H3N2 and B/Victoria from Southeastern Asia to temperate regions for the pandemic seasons and the interpandemic period (after removing outlier seasons and aligning at the median peak). Grey lines show viral movement events for each season in the interpandemic period after epidemic alignment; cyan-blue is the interpandemic average, orange the A/H1N1 pandemic season and red the COVID-19 pandemic season. ISO week 53 was removed for some years to maintain temporal consistency. The scale of relative values is comparable between (**c**) and (**d**).

been newly introduced or persisted in the region from a previous season. Briefly, for lineages in Southeastern Asia, "persistent lineages" are defined as those lineages descended from the most recent Southeastern Asia trunk node. Although we do not interpret this in terms of epidemiological persistence of transmission chains between seasons, these lineages can be seen as more likely to have persisted from previous seasons rather than being recently introduced into Southeastern Asia (Fig. 3a, details in "Methods").

The maximum clade credibility (MCC) tree of A/H3N2 exhibited a trunk that was consistently associated with Southeastern Asia, whereas the trunk location of B/Victoria displayed variations across influenza seasons (Fig. 3b, c, Supplementary Fig. 9), consistent with more balanced B/Victoria fluxes between Southeastern Asia and temperate regions (Fig. 2a, b). This aligns with past observations that global A/H3N2 circulation patterns exhibit a stronger and more predictable source-sink dynamic than B/Victoria[4,26,27]. We found that a

higher percentage of A/H3N2 viruses sequenced in Southeastern Asia belonged to persistent lineages (86.1%) than B/Victoria viruses (36.3%) ($P < 0.001$, chi-square test) (Fig. 3d, e). Interestingly, the percentage of A/H3N2 viruses in Southeastern Asia belonging to persistent lineages appears to have increased during the COVID-19 pandemic season (Fig. 3d). These findings remain robust to the sub-sampling schemes (Supplementary Fig. 10).

Shifts in antigenically leading and trailing patterns
To provide more insights into the evolutionary heterochrony across regions and seasons, we calculated sequence-based antigenic distances for A/H3N2, a subtype whose antigenic sites have been clearly resolved[28,29]. Based on the HA genetic sequence of A/H3N2, we calculated the Hamming distances of each virus strain to the vaccine strain (A/Wisconsin/67/2005) across the five major antigenic sites following the approach from[30]. We found that A/H3N2 viruses evolved linearly
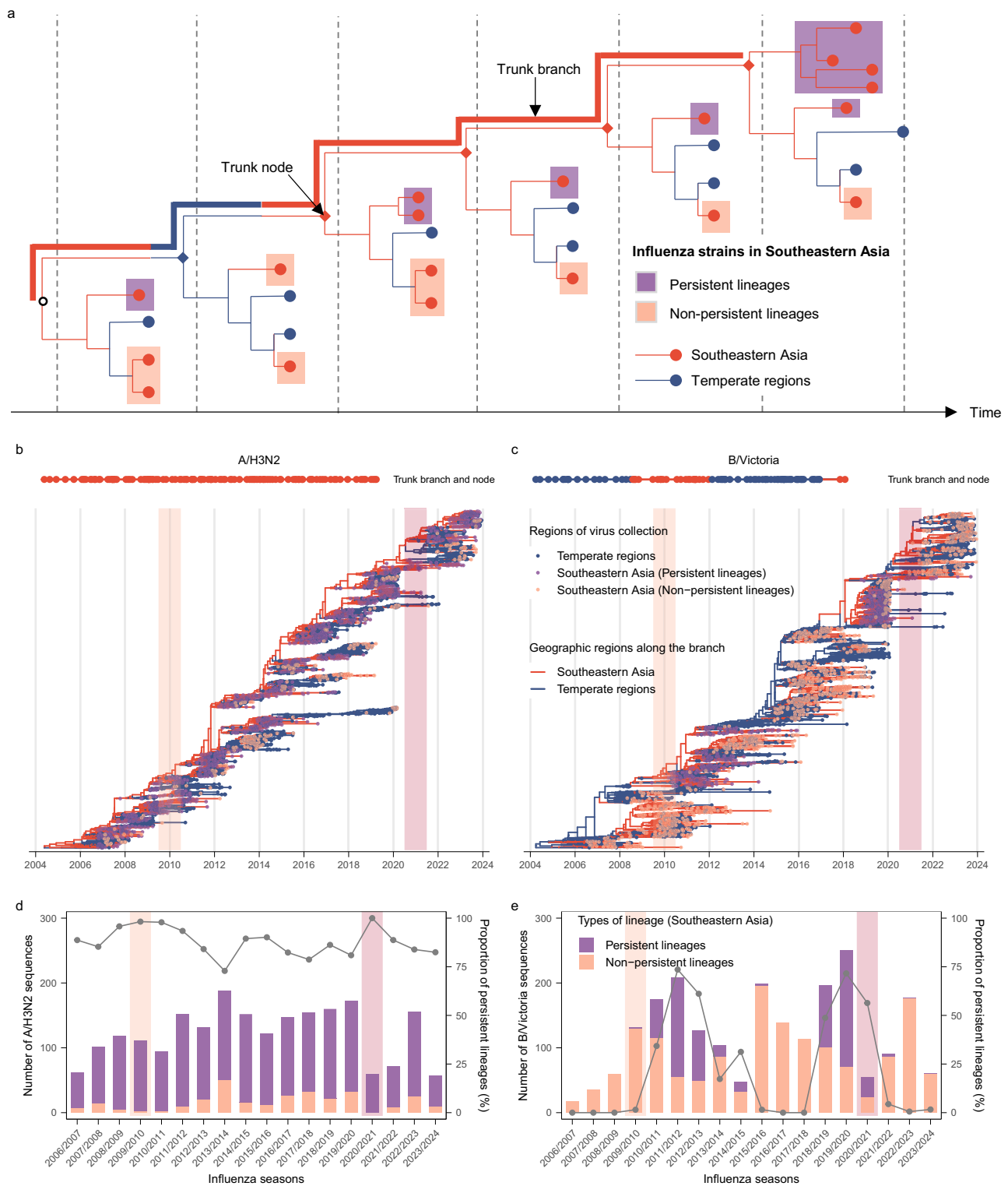
Fig. 3 | Persistent lineages within Southeastern Asia and their topological and temporal distributions under the even sub-sampling scheme. a Schematic diagram illustrating how viruses circulating in Southeastern Asia belonging to persistent lineages were identified. A Southeastern-Asia tip was defined as belonging to a persistent lineage if its nearest trunk node was associated with "Southeastern-Asia" and all ancestor nodes from this tip to the nearest trunk node were associated with "Southeastern-Asia" backwards in time. Trunk was defined as all branches ancestral to viruses sampled within 1 year of the most recent sample. **b**, **c** The maximum clade credibility (MCC) tree of A/H3N2 and B/Victoria lineages. Tips are coloured by geographic region of virus collection, in which strains in Southeastern Asia are separately annotated as belonging to persistent or non-persistent lineages; internal branches are coloured by geographic region as inferred by Bayesian phylogeographic methods. Trunk nodes over time are presented as dots coloured by trunk location on a horizontal line at the top of the panels. Trunk assignments are summarised up to the most recent common ancestor (tMRCA) of viruses sampled within 1 year of the most recent sample. **d**, **e** The temporal distribution of the numbers of sub-sampled virus genomes from Southeastern Asia belonging to persistent and non-persistent lineages over influenza seasons, for A/H3N2 and B/Victoria lineages, respectively (left y-axis). The proportion of virus sequences belonging to persistent lineages over time is represented by the grey line (right y-axis).
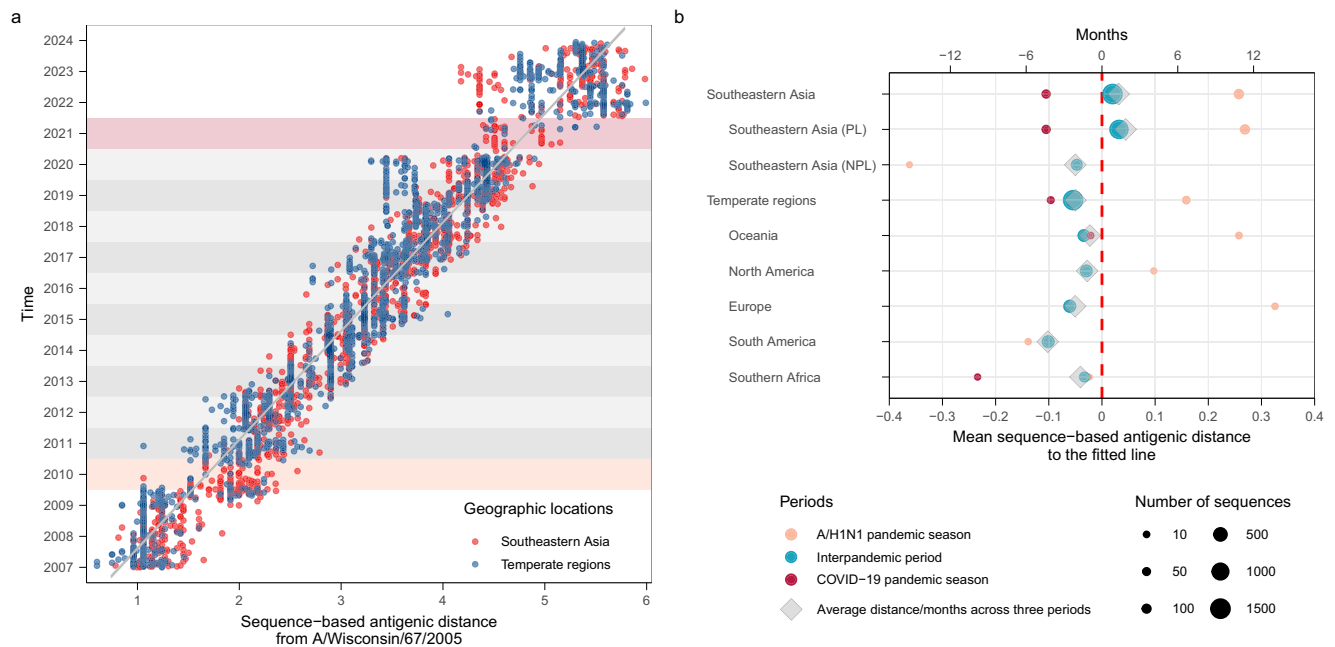
Fig. 4 | Leading and trailing geographic regions of A/H3N2 antigenic evolution under the even sub-sampling scheme. a Sequence-based antigenic distance from A/Wisconsin/67/2005 of all A/H3N2 virus strains plotted against time of collection. The thick grey line is the fitted line using a linear model. Points to the right of the line are antigenically advanced, whereas strains to the left of the line are antigenically lagging. Light and dark red shading denotes the A/H1N1 and COVID-19 pandemic seasons, respectively. **b** Antigenic distance to the fitted line by region and period. Grey oblique squares indicate the average antigenic distance to the fitted line for strains isolated in each region. Coloured circles split this overall average by various periods (2009 H1N1 pandemic, interpandemic, and COVID-19 pandemic seasons). Size of circles refers to the number of sequences that are used for the estimate. Points to the right of the graph are antigenically advanced, whereas strains to the left are antigenically lagging. Antigenic distance can also be interpreted as time using the slope of the regression line in panel **a**; thus, time is shown as a second x-axis (top). The absence of observations in certain periods is attributed to incomplete gene sequences, making it challenging to compute antigenic distance. PL persistent lineages, NPL non-persistent lineages.

from 2007 to 2023 (Fig. 4a), with no clear outliers during the pandemic seasons. This suggests that A/H3N2 viruses circulating in both Southeastern Asia and temperate regions underwent antigenic evolution in a globally homogeneous way, consistent with the ladder-like tree topology of A/H3N2 (Fig. 3a) and previous findings[4,31].

Next, we explored which regions typically lead or lag A/H3N2 antigenic evolution, and whether pandemics may have disrupted these patterns. We computed the distance of each strain to the fitted line between antigenic distance and time of collection, for which points to the right of the line indicated antigenically advanced strains, while those to the left indicated antigenically lagging strains[4] (Fig. 4a). During the interpandemic period, newly emerged A/H3N2 strains appeared in Southeastern Asia on average, 3.1 months earlier than in temperate regions, while the greatest lag in arrival of antigenic novelty was found in South America with a delay of 5.1 months (Fig. 4b). Within Southeastern Asia, persistent A/H3N2 strains appeared on average 3.3 months earlier than non-persistent lineages. Additionally, this leading and trailing pattern differed from period to period (Fig. 4b). During the A/H1N1 pandemic, newly emerged A/H3N2 strains appeared on average 10.0 months earlier in Southeastern Asia and 9.0 months earlier in temperate regions compared to the interpandemic period (both $P < 0.001$, Supplementary Table 3). However, during the COVID-19 pandemic, A/H3N2 antigenic evolution lagged in both Southeastern Asia (by 5.3 months, $P < 0.001$) and temperate regions (by 1.8 months, $P = 0.632$) compared to the interpandemic period (Supplementary Table 3).

We also used genetic distance to perform the same analysis for B/Victoria, motivated by congruent patterns between antigenic distance and genetic distance for A/H3N2 (Fig. 4, Supplementary Fig. 11a, b). Compared to A/H3N2, in Southeastern Asia, the time-advanced pattern of B/Victoria during the interpandemic period is absent, while the advanced pattern (by 8.5 months) during the 2009 H1N1 pandemic is

still observed, and the lagged pattern (by 4.5 months) during the COVID-19 pandemic is only observed for persistent lineages (Supplementary Fig. 11c, d). More population-based and modelling studies are required to deepen our understanding of the exact mechanisms underpinning our observations.

Characterising the A/H3N2 movement network within Southeastern Asia

Next, we used the persistent lineages of A/H3N2 within Southeastern Asia, identified earlier, to reconstruct the transmission network in this region. Although the inferred internal network fluctuated from season to season, we constructed an average network using the intensity of viral movement between pairs of sub-locations per season during the interpandemic period as a baseline, and contrasted baseline patterns with those of pandemic seasons (Fig. 5a). During the A/H1N1 pandemic, the overall number of inferred virus movement events declined by 52.2% compared to the baseline, whereas movement intensity increased for routes from Indonesia-East Timor and Laos (Fig. 5b, Supplementary Fig. 12). During the COVID-19 pandemic, the overall number of viral movements declined by 85.3% compared to the interpandemic period (Fig. 5c). The reductions were consistent for the epoch-specific dispersal rates accounting for the tree length (decreased by 53.5% and 69.7% during the 2009 A/H1N1 and COVID-19 pandemic seasons, respectively) (Fig. 5d). We further subdivided Southeastern Asia into East Asia, South Asia, and Southeast Asia to perform a multidimensional scaling analysis for vectorized asymmetric movement matrices among these three sub-regions. There was a marked divergence in internal movement network structure during the COVID-19 pandemic, and to a lesser extent during the A/H1N1 pandemic season, in comparison to the well-mixed pattern that was observed during the interpandemic seasons (Fig. 5e). Further analysis of the trunk location revealed a temporally varying pattern
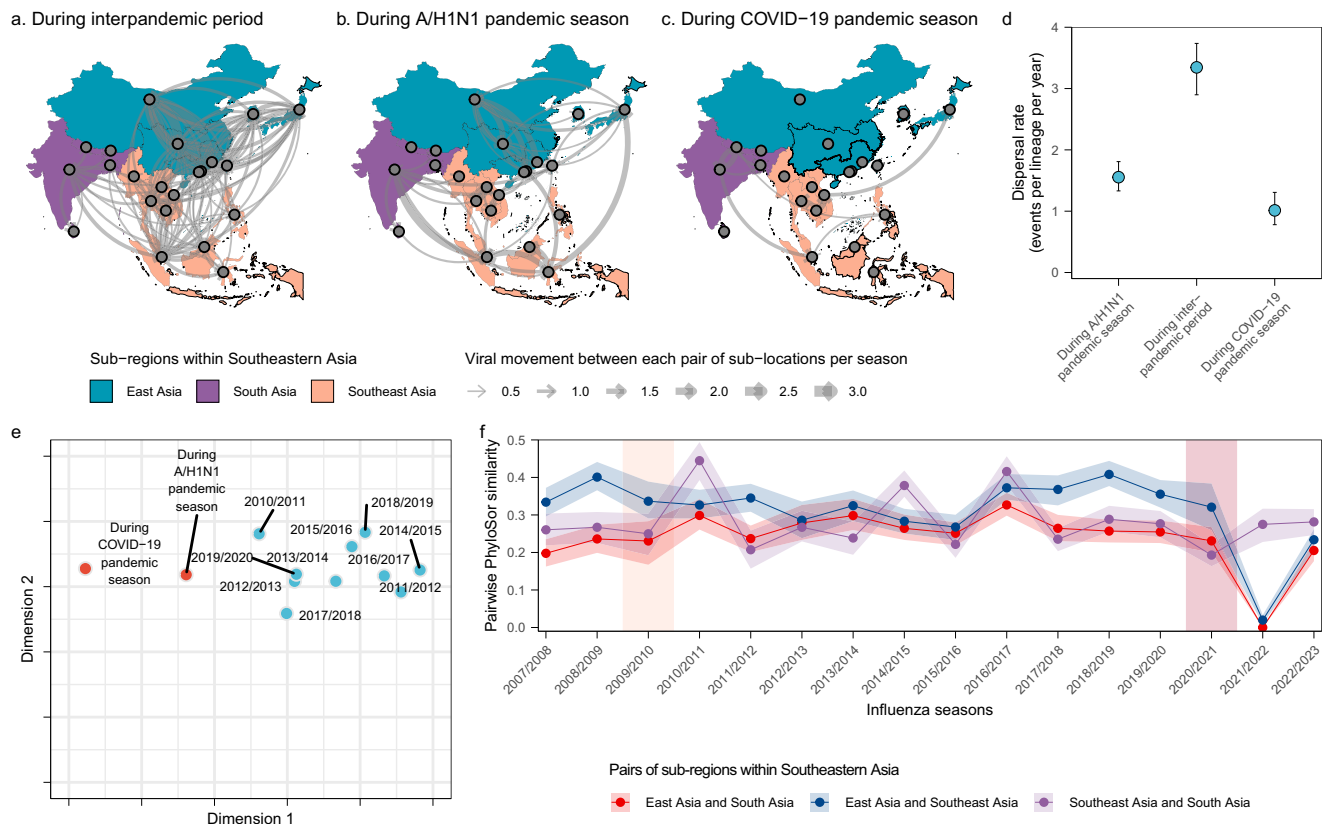
Fig. 5 | The migration network and phylogenetic similarity of persistent A/ H3N2 strains within Southeastern Asia. a–c The average viral movement events between pairs of sub-locations per season during the three periods. Only lines representing a number of viral movement events greater than 0.5 per season are shown, for clarity. Three sub-regions within Southeastern Asia are coloured, where East Asia encompasses China, Japan, and South Korea, and South Asia includes Bangladesh, Bhutan, India, Sri Lanka, and Nepal. **d** Period-specific dispersal rates inferred during the phylogeographic reconstruction. Posterior mean estimates (filled circles) with 95% HPD intervals (error bars) are shown, based on a total of 450 post-burnin samples. **e** Multidimensional scaling analysis for vectorized asymmetric jump matrices among the three sub-regions (East Asia, South Asia, and Southeast Asia) in different influenza seasons. **f** Pairwise PhyloSor similarity of virus strains circulating between pairs of sub-regions within Southeastern Asia over influenza seasons as a proxy for lineage mixing. The smaller the Pairwise PhyloSor similarity is, the less mixed the lineages circulating between pairs of sub-regions are. Data are presented as mean values (points) with 95% HPD intervals (shaded areas around the lines).

(Supplementary Fig. 13), indicating that the internal network within Southeastern Asia is a dynamic process that is maintained not only by one sub-location as the source population, consistent with prior work[4].

We further estimate the A/H3N2 phylogenetic similarity using the tree topology and branch length[32] (PhyloSor, details in "Methods"), as a proxy for lineage mixing among the three sub-regions (East Asia, South Asia, and Southeast Asia). During the A/H1N1 pandemic season, there was a considerable amount of lineage mixing between pairs of sub-regions within Southeastern Asia, aligned with that of prior seasons, but a notable increase was seen in 2010–2011 between Southeast Asia and South Asia (similarity: 0.44, 95% highest posterior density (HPD): 0.39–0.49, Fig. 5f). The extent of lineage mixing only slightly declined during the COVID-19 pandemic season in 2020–2021 for all pairs of sub-regions, but declined precipitously in 2021–2022 between East Asia and South Asia, and East Asia and Southeast Asia. We hypothesise that virus lineages are still able to circulate on the same branch of a tree phylogeny despite low activity, explaining the "delayed" effect of the pandemic on A/H3N2 similarity. To test this, we further investigated viral movements in East Asia, where we selected China as an example to assess the impact during and after the adoption of stringent border closures. We found that overall airline traffic into and out of China correlated well with viral movement fluxes into and out of China (Pearson correlation coefficient: 0.91 and 0.93, respectively). However, the internal viral movement intensity in China recovered earlier and to a larger extent than cross-border movement from/to China, after

border control measures were gradually relaxed in the 2021–2022 season (Supplementary Fig. 14).

Finally, we show that the time-variable air traffic network among pairs of sub-locations strongly contributed to the internal A/ H3N2 spread within the whole Southeastern Asia region for the entire period (coefficient: 0.95, 95% HPD: 0.81–1.12, Supplementary Table 4). Our results also indicate a positive association between overall dispersal rate and the total airline traffic (log regression coefficient: 0.44, 95% HPD: 0.32–0.57).

Discussion
We expanded and refined our previous work[10] by focusing on Southeastern Asia and comparing two distinct pandemics (strong decline in human movements during the COVID-19 pandemic, pronounced pathogen interference during the A/H1N1 pandemic) at a finer spatiotemporal resolution. We demonstrated that typical autumn-winter waves of A/H3N2 and B/Victoria movements from Southeastern Asia to temperate regions disappeared almost completely during the COVID-19 pandemic-related disruption. However, B/Victoria lineage movement into temperate regions still occurred during the A/H1N1 pandemic. While we observed a wave of B/Victoria exports from Southeastern Asia to temperate regions during the A/H1N1 pandemic, coinciding with a large B/Victoria epidemic wave in Southeastern Asia, these exports did not spark B/Victoria epidemic waves in temperate regions, suggesting little to no establishment of exported lineages.

We found opposite patterns of pandemic-related disruptions on A/H3N2 antigenic evolution. The time-advanced pattern of A/H3N2 antigenic evolution seen globally during the A/H1N1 pandemic may be linked to modest NPIs and enhanced natural selection from competition with intense circulation of A/H1N1pdm09 worldwide. Conversely, the lagged pattern of A/H3N2 evolution seen in Southeastern Asia during the COVID-19 pandemic could be attributed to limited influenza circulation and evolution due to human behavioural changes driven by stringent and long-lasting NPIs. Additionally, a higher proportion of A/H3N2 lineages circulating within Southeastern Asia have been estimated to persist across seasons as compared to B/Victoria lineages. By analysing those persistent lineages, we highlight how the A/H3N2 internal migration network within Southeastern Asia is characterised by a dynamic change in trunk locations over time. During the COVID-19 pandemic season, it was shaped by reductions in the intensity of inferred viral movements, the diverse structure of the internal movement network, and decreased lineage mixing. Changes in the circulation network within Southeastern Asia were less pronounced during the A/H1N1 pandemic season likely due to fewer pandemic-related disruptions at that time.

We extended previous work[4,26,27] to consider a broader geographic scope of Southeastern Asia and characterise the main trunk location for the global influenza circulation. Our data suggest that Southeastern Asia plays a more conspicuous role in the global circulation of A/H3N2 compared to B/Victoria. The importance of Southeastern Asia in the evolution of A/H3N2 has been further attributed to the seasonal nature of influenza in temperate regions, in which strong genetic and transmission bottlenecks lower the likelihood of local persistence and global fixation of circulating strains[14,33]. However, the internal network maintaining the leading role of Southeastern Asia has rarely been explored in a quantitative manner[4]. Our quantitative analyses reveal that the movement network within Southeastern Asia is characterised by highly connected dispersal routes among the major airline transportation hubs (Supplementary Fig. 12a) and a temporally varying trunk location (Supplementary Fig. 13). This network of asynchronous but temporally overlapping epidemics, connected by proximity and human mobility, promotes antigenic evolution and global dispersal of A/H3N2 strains. In contrast, global B/Victoria circulation exhibits less dependence on Southeastern Asia, with a pattern of geographically separate evolution and circulation rather than global dispersion, consistent with a previous study[26]. Although the underlying mechanisms driving the heterogeneity across viruses remain unclear, we speculate that the more rapid antigenic drift for A/H3N2 compared to B/Victoria[34] could potentially result in a greater intrinsic fitness advantage. Additionally, it has been suggested that younger ages of infection for B/Victoria compared to A/H3N2 could lead to less spatial dissemination as children are less mobile than adults[26,35].

Influenza circulation patterns are also subject to alteration via changes in human behaviour, especially mobility, during pandemics. The occurrence of two global pandemics (2009 A/H1N1 and COVID-19) in the 21st century has provided a natural experiment for evaluating changes in human mobility and immunity and their impact on influenza transmission at the population level (we did not consider other large epidemics/outbreaks, such as Zika virus, as they were localised to specific parts of the world). Differences in the circulation and evolutionary patterns of influenza viruses during the two pandemics can be interpreted by a complex interaction between local NPIs, regional and global mobility, and viral interference. In addition to the higher intensity and duration of NPIs during the COVID-19 pandemic, human behavioural changes including contact reduction and mask wearing will have also contributed to the decline of respiratory infections during the COVID-19 pandemic[36]. Accordingly, perturbation of influenza virus circulation was more drastic during the COVID-19 pandemic, coinciding with our findings where most internal transmission within Southeastern Asia was halted. Although we could not study the B/

Yamagata lineage in this work, the global potential elimination of this lineage from surveillance data in late 2020 attests to the marked perturbation of the COVID-19 pandemic period on global influenza dynamics[37].

The novelty of our approach is to contrast the pronounced perturbation of the COVID-19 pandemic with a pandemic of a more moderate kind, the 2009 A/H1N1 pandemic, which we hypothesised would have also affected circulation patterns of resident influenza strains. The novel virus responsible for the 2009 A/H1N1 pandemic is thought to display viral interference with seasonal influenza A viruses, presumably via more specific heterosubtypic cross-immunity[6,38]. Since A/H3N2 viruses are more closely related to A/H1N1pdm09 viruses than B/Victoria viruses, massive circulation of A/H1N1pdm09 in the first pandemic wave may have limited the circulation and diffusion of A/H3N2 viruses via competition for susceptibles, in line with a consistent globally negative correlation between influenza A/H3N2 and A/H1N1pdm09 activity[23]. This competition was further illustrated in our analysis by the disappearance of the second A/H3N2 peak wave and A/H3N2 movement wave from Southeastern Asia to temperate regions during the A/H1N1 pandemic season. In contrast, we see few changes in influenza B/Victoria circulation, consistent with less or no cross-immunity. NPIs could have also played a role during the A/H1N1 pandemic disruptions from the perspective of air travel controls in our study (Supplementary Figs. 3, 15), although NPIs (e.g., school closures) were limited to a few countries and the early weeks of the pandemic[39]. Lastly, variations in pre-existing population immunity prior to the onset of a pandemic might also contribute to differences in influenza circulation observed during two pandemic periods[40]. Disentangling the roles of NPIs, viral interference, immunity, and other potential factors in shaping the circulation patterns of seasonal influenza merits more investigation.

These findings have several public health implications. First, seasonal influenza epidemics occur each year while pandemics only occur sporadically, thus interactions between seasonal respiratory pathogens and pandemics are also likely to occur in the future. Understanding the circulation patterns during these two pandemics may enhance preparedness against influenza outbreaks in interpandemic seasons and when facing future public health emergencies. Future work should model the impact of different types of interventions on the dynamics of seasonal influenza both in Southeastern Asia and globally to guide mitigation strategies. Second, temporally varying trunk locations within Southeastern Asia support the need for geographically extensive virological and genomic surveillance in this region, allowing for earlier identification of antigenically novel strains and thereby providing a longer lead time for developing and rolling out effective vaccines. A strong collaboration between WHO South-East Asia and WHO Western Pacific regions remains vital to maintain a high surveillance intensity across Southeastern Asia that in turn enhances pandemic preparedness. Third, the complex internal dispersal network in Southeastern Asia highlights the importance of country-specific vaccination strategies against seasonal influenza (e.g., vaccine strain and vaccination timing)[17], in particular in the context of altered seasonality and interrupted vaccination rollout during and after the pandemic. Establishing a global influenza migration network at a finer geographic scale (e.g., country level; over 120 WHO Member States have contributed to influenza surveillance as of May 2024[41]) also holds promise for optimising vaccine recommendations tailored to each country's future influenza outbreaks. Fourth, a new pandemic may reshape the landscape of influenza invasion and co-circulation based on ecological coexistence theory[42]. Further, changes in human-animal contact, the human-environment interface, and climate conditions could influence the viral evolution and emergence of novel influenza strains. Integrating ecological and social processes into activities of surveillance networks helps us better understand the drivers of influenza circulation and evolution.

Our results should be interpreted in the context of several limitations. First, inherent biases exist due to the nature of genetic data from heterogeneous genomic surveillance efforts and data-sharing initiatives worldwide. To address these issues, we carefully down-sampled genetic data geographically and temporally; our main conclusions are robust across various sets of genetic data from different sub-sampling schemes (Supplementary Figs. 8–10 and 16). Nevertheless, we acknowledge that our dataset completely omits data from large and populous parts of the world (e.g., West, Central and East Africa, Central America, Russia etc.) that could potentially play important roles in the global influenza network. However, our aim is not to reconstruct the global spread of seasonal influenza viruses, but rather to focus on the network within Southeastern Asia and the role of Southeastern Asia in seeding epidemics in temperate regions. Secondly, we recognize that the implementation and lifting of NPIs varied across locations and time, and thereby the impact of these changes on influenza circulation patterns may be heterogeneous—here we concentrate on regional averages. For simplicity, our study considered the same pandemic period definition for all countries although NPIs were put in place in a heterochronous way. In addition, the influenza season defined in this study did not uniformly align well with that in the Southern Hemisphere due to the asynchronous influenza circulation worldwide. Third, epidemic alignment of influenza activity and movement across seasons could be affected by some atypical seasons, but we believe that the average multi-year curves enable us to capture baseline seasonality patterns. Lastly, our study only retrospectively tracked the patterns of influenza circulation over a long-term period, without dissecting the contribution of behavioural and immunological factors. For example, the impact of domestic and international public health measures on viral evolution and diversity should merit more mechanistic investigation. However, we believe that the present findings could guide more causal analyses in the future.

In summary, our study provides a comprehensive reconstruction of the circulation patterns of seasonal influenza viruses both out of and within Southeastern Asia during the 2009 A/H1N1 and COVID-19 pandemics with comparison to the interpandemic period. We highlighted the heterogeneous impact of two distinct pandemic-related disruptions on evolution and mixing of seasonal influenza, focusing on the transmission dynamics within Southeastern Asia. Our empirical findings can help anticipate the effects of adopting control measures as routine practices to mitigate the disease burden of seasonal influenza, as well as preparedness against outbreaks of influenza or other seasonal respiratory pathogens in future pandemic scenarios.

Methods

To develop our methods for epidemiological and genomic assessment, we combined epidemiological, genetic and airline data, together with a phylodynamic framework to infer viral movements and the emergence of antigenic novelty at various spatial levels.

Epidemiological data

Global virological surveillance data for seasonal influenza was retrieved from FluNet, based on the WHO-led Global Influenza Surveillance and Response System (GISRS)[41] and collated according to the methodology followed in ref. 10. We extracted the weekly number of specimens processed for influenza testing and positive detections by subtypes or lineages to calculate weekly positivity rates. We defined the influenza season in the southern hemisphere as running from ISO week 1 to week 52 of one year, whereas the influenza season in other regions was defined as running from ISO week 27 of one year to ISO week 26 of the next year. In each region, we defined an average seasonal pattern for interpandemic seasons based on the total positivity rates p_{ij} of each seasonal influenza virus subtype/lineage in week i during influenza season j. We averaged the positivity rates p_{ij} across interpandemic seasons after aligning curves based on the median week

of peak occurrence with outlier seasons removed (for details see Supplementary Figs. 1, 2)[21,43]. Since Southeastern Asia experienced two yearly A/H3N2 waves during interpandemic seasons we performed two epidemic alignments per season by splitting each influenza season into a summer (ISO week 14–39) and winter season (ISO week 40 to ISO week 13 of the next year).

Air traffic data and compound airline traffic indicator

Airline passenger booking data from January 2011 to December 2023 were accessed from Official Airline Guide (OAG) Ltd. through a data sharing agreement. Since no airline passenger data were available before 2011, we used the airline capacity data (the number of seats) from OAG instead, and assumed a proportional relationship with the number of passengers travelling[2] (Supplementary Fig. 15). We refer to both measures as airline traffic hereafter.

To obtain a proxy stringency index for the H1N1 pandemic, we first examined the relationship between the COVID-19 stringency index and airline traffic during the COVID-19 pandemic for each sublocation in Southeastern Asia (Supplementary Table 2). Given the COVID-19 stringency index is a composite measure of nine response metrics, including internal movements, international travel controls, and other human behavioural changes[44], we could only construct an air travel-related stringency index (compound airline traffic indicator) by considering both the within-sublocation airline traffic and international airline traffic from/to each sublocation. This indicator did not cover other types of behaviours and policies beyond air travel, which should reflect part of the extent of NPIs. Note that since there is no internal airline traffic in Hong Kong (China), Macao (China) and Singapore, we constructed an indicator with only air travel from/to the sublocation for these three sublocations. In each sublocation, for each airline traffic indicator (domestic or international), we compared the change relative to the same month in 2019 (referred to as the baseline month). The baseline month represents a normal value for that month before the COVID-19 pandemic. Monthly baselines were used because of seasonal fluctuations in airline traffic. The composite indicator using airline traffic is then given by

$$100 - (\text{Relative value}_{\text{domestic}} + \text{Relative value}_{\text{international}}) \times 50$$

and serves as a proxy air travel-related stringency index. The indexes that are below zero are set to zero. Because of the strong correlation between the compound airline traffic indicator and the COVID-19 stringency index (Supplementary Table 2, Supplementary Fig. 3), we use the compound airline traffic indicator to also define an air travel-related stringency index for the H1N1 pandemic, using airline traffic in 2008 as a baseline.

Statistical analysis

We used the Variable Selection Using Random Forests (VSURF) algorithm to determine the predictors associated with the influenza activity decline during the two pandemics, respectively[45,46]. We calculate the positivity rate of influenza A/H3N2 and B/Victoria among specimens by quarter (three-month intervals) in each sublocation (0.5 positive cases are added to avoid division by zero issues). In each sublocation, quarters with fewer than 20 tested specimens are removed. To control for seasonality, we computed the ratio of influenza positivity rate relative to the baseline quarter level during the pre-pandemic period, and then log-transformed the ratios. Baseline quarter represents an average value for that quarter in the years 2004–2008 or 2015–2019, respectively. The variables included in the model contained sub-location-specific factors (population density, age, latitude, absolute humidity, temperature, socio-demographic index), and pandemic-related factors (COVID-19 or air traffic-related stringency index, pandemic case incidence). Demographic data were downloaded from 2024 Revision of World Population Prospects[47], and

the details of other data sources are presented in Supplementary Table 1. We rank the variables according to a variable importance measure, where importance is defined as the increase in prediction error when the variable of interest is randomly reshuffled across observations[45,46].

Collation and sub-sampling of viral sequence data

We focused on A/H3N2 and B/Victoria in this study, because A/H1N1pdm09 only emerged in 2009 and therefore cannot be regarded as a seasonal influenza virus during the 2009 pandemic season[19], and B/Yamagata was potentially eliminated after March 2020[20]. A global genetic dataset of seasonal influenza sequences (hemagglutinin (HA) segment) sampled between 2007 and 2023 was retrieved from GISAID and GenBank on 17 Jan 2024, with details of data processing in[10]. In brief, we performed data quality assessment, deduplication, aggregation, and cleaning steps. To retain more sequences than our previous study[10], we also included sequences with incomplete collection dates and only discarded poor quality sequences, as defined by the quality control criteria in Nextclade[48,49].

Geographic locations of sequences were classified into Southeastern Asia and temperate regions, according to previous understanding of the global influenza circulation network[4]. Based on previous work on transmission characteristics of influenza and availability of genetic data in Asia[16,26], here we defined the geographic scale of "Southeastern Asia" as comprising the entirety of Southeast Asia, parts of East Asia (China, Japan, South Korea), and parts of South Asia (Bangladesh, Bhutan, India, Sri Lanka, Nepal), which is in line with one of the seven influenza transmission zones defined in a previous clustering analysis[16].

To trace the internal transmission network of influenza within Southeastern Asia, we used finer-grained internal spatial demes (Supplementary Fig. 7), where the majority of demes are set at country levels. Further, we divided mainland China into three zones, based on previous work showing heterogeneous seasonality patterns driven by climatic conditions (winter peak in north China, semi-annual peaks in central China, and spring peak in south China)[50,51]. In addition, in China, we separated Hong Kong, Macao, and Taiwan due to their distinct positions in the global air transport network[52] and heterogeneous non-pharmaceutical interventions (NPIs) adopted during both pandemic interruptions compared to mainland China[53]. Finally, we combined Indonesia and East Timor, as well as Malaysia and Brunei, due to the low availability of publicly available genetic data in these neighbouring countries. This resulted in a total of 22 "country/sub-location level" (referred to as sub-location level hereafter) demes within Southeastern Asia.

Temperate regions comprised five sub-regions: North America (Canada and USA only) and Europe (Russia excluded) in the northern hemisphere (NH); Oceania (Australia and New Zealand only), South America, and the Southern part of Africa in the southern hemisphere (SH) (Supplementary Fig. 7). The entirety of South America was classified as a Southern Hemisphere temperate zone, given the recommended use of the Southern Hemisphere vaccine formulation throughout the region[54] and a similar seasonality pattern across the whole region[5]. We recognize that tropical land masses exist in the northern part of South America.

To reduce the impact of sampling biases while maintaining computational feasibility, we carefully sub-sampled the global sequence dataset. For each subtype/lineage, we designed three subsampling strategies to select ~6000 HA sequences collected from January 2007 to December 2023, of which half (~3000) were allocated to Southeastern Asia. In the first sub-sampling scheme (even sub-sampling, main analysis), we sub-sampled equal numbers of sequences per sub-location per year (where available) in Southeastern Asia. In temperate regions, we first allocated ~600 sequences for each sub-region where available, and then sub-sampled

equal numbers of sequences per sub-location per year. The second sub-sampling scheme selected sequences proportional to human population. Specifically, we set the number of sequences for each sub-location proportional to the sub-location-specific population size (with a minimum number of 100 sequences per sub-location) in Southeastern Asia; in temperate regions, we first set that number proportional to population size for each sub-region (with a minimum number of 300 sequences per sub-region), and then sub-sample equal numbers of sequences per sub-location per year within each sub-region. We sub-sampled equal numbers per year, because more recent years are overrepresented in sequence numbers compared to previous years (Fig. 1f, j). Sequences selected in the third subsampling scheme were proportional to the product of population size and influenza positivity rate binned by ISO year. Throughout, among the smallest sub-sampling units (per sub-location per year), more sub-sampling weights were given to sequences with more complete collection dates and higher quality sequences.

Phylogenetic analyses

We aligned sequences in the sub-sampled datasets in Nextclade and only kept the coding regions[48]. We then constructed maximum likelihood (ML) phylogenies using IQ-TREE2[55]. The resulting phylogenetic trees were inspected in TempEst to identify and remove temporal outliers[56]. To better manage the number of sequences, we further reduced clades of sequences where all sequences originated from a single sub-location to a single representative sequence, since such clades contain no information about transitions across sub-locations. This subsampling process resulted in reducing the datasets to ~4000 genetic sequences.

The ML tree was re-estimated for the reduced genetic datasets using the same specifications described above. We then inferred the time-calibrated tree using TreeTime[57], which served as the starting tree for Bayesian phylogenetic inference. Phylogenetic trees were inferred in a Bayesian framework using BEAST v1.10.5[58] and the high-performance BEAGLE library[59], in which we incorporated a starting ML tree, a HKY nucleotide substitution model with gamma-distributed rate variation among sites, and a constant coalescent prior using a Hamiltonian Monte Carlo (HMC) kernel on the population size and node heights. The simple constant coalescent prior was chosen to manage the computational burden. A strict molecular clock model was adopted due to the strong correlations between root-to-tip genetic distance and collection date (minimum Pearson correlation coefficient among all datasets: 0.95) (Supplementary Fig. 17). Samples with incomplete dates had dates of sampling estimated assuming a uniform prior within the known temporal bounds. These analyses were run for 400–600 million MCMC steps for three chains and sampled every 100,000 steps, with the first 10%-15% considered as burn-in.

Phylogeographic analyses

Two-state phylogeographic analysis. Using the posterior set of trees from the above phylogenetic analyses as a set of empirical trees, we performed a two-state time-inhomogeneous asymmetric discrete trait analysis (DTA) in BEAST 1.10.5, where sequences collected from Southeastern Asia and temperate regions were labelled based on their respective geographic deme. We used the epoch extension to specify five epochs where each epoch spans a single or multiple influenza seasons: i) before the A/H1N1 pandemic season (before 30 June 2009), ii) A/H1N1 pandemic season (from 1 July 2009 to 30 June 2010), iii) interpandemic period (from 1 July 2010 to 30 June 2020), iv) COVID-19 pandemic season (from 1 July 2020 to 30 June 2021), and v) after the COVID-19 pandemic season (after 1 July 2021), enabling us to account for variations in migration rates. Individual counts of transitions between demes were estimated in the form of Markov jumps and rewards[60].

Identifying persistent lineages. We identified those Southeastern Asia virus strains that directly descended from the Southeastern-Asia trunk node of the trees, where the trunk was defined as all branches ancestral to viruses sampled within 1 year of the most recent sample[26]. We referred to those lineages as "persistent lineages", which can be considered as roughly equivalent to the opposite of the "transmission lineages" defined in[61]. To achieve this, in brief, we first initiated a depth-first search from each Southeastern-Asia tip for each tree in posterior samples. We defined the Southeastern-Asia tip as belonging to a persistent lineage in this tree if the trunk node from which it descends was associated with "Southeastern-Asia" and also all ancestor nodes in the path from tip to this trunk node were associated with "Southeastern-Asia" as well (Fig. 3a). We then summarised the distribution of "persistent lineages" for the posterior set of trees, for which those tips that are classified as belonging to persistent lineages in more than 50% of the posterior tree samples would be ultimately labelled as belonging to "persistent lineages".

Internal GLM-diffusion phylogeographic analysis. The internal movement network within Southeastern Asia was inferred using only sequences classified as belonging to persistent lineages in the prior analysis under the even sub-sampling scheme. As this involved a more manageable number of sequences, we inferred the phylogenetic trees of persistent lineages in BEAST v1.10.5 with a parameter-rich setting where we specified an SRD06 nucleotide substitution model[62], a Bayesian Skygrid coalescent prior (with grid points equidistantly spaced in six-month intervals)[63], and a strict molecular clock model. Using the posterior trees from this analysis as empirical trees, we performed a time-inhomogeneous phylogeographic model with a generalised linear model (GLM) to parameterise the migration rates among the 22 Southeastern Asia sub-locations defined above, with Markov jumps and rewards logged to estimate the transition events[60]. Both overall and relative migration rates were set to be epoch-specific, using the same epochs as above. We collated, aggregated, and standardised time-inhomogeneous airline traffic volumes in the five epochs[10]. The airline data of the five epochs refers to i) airline capacity from January 2007 to June 2009; ii) airline capacity from July 2009 to June 2010; iii) airline passenger volumes from January 2011 to June 2020; iv) airline passenger volumes from July 2020 to June 2021, and v) airline passenger volumes from July 2021 to December 2023, respectively. Covariate was incorporated in the phylogeographic GLM model, assuming time-homogeneous effect sizes and inclusion probabilities[64]. Furthermore, we also extend the model by adding a time-inhomogeneous overall rate scaler to accommodate temporal variation in overall airline traffic (air capacity data were used as they are available from 2007 to 2023) as a predictor of the overall migration rates[64].

Summary of posterior trees. We used the TreeMarkovJumpHistoryAnalyzer tool to obtain posterior summaries of all Markov jump counts (referred to as viral movement events) from posterior trees[64]. In terms of viral movements from Southeastern Asia to temperate regions, we averaged the weekly movement intensity per season after aligning the movement time series based on the median peak weeks for the seasons during the interpandemic period, with the outlier seasons (e.g., no peak in that season) removed[21,43]. The procedure followed is similar to the methodology illustrated in Supplementary Figs. 1 and 2.

For A/H3N2 persistent lineages circulating within Southeastern Asia, we estimated the PhyloSor similarity between each pair of three sub-regions (East Asia, South Asia, and Southeast Asia) in Southeastern Asia, which quantifies the similarity of viral populations between those locations as the proportion of branch lengths in phylogenetic trees that are shared relative to the total branch lengths of both populations[32]. Additionally, we computed Euclidean distances among

seasons for those vectorized asymmetric jump matrices among three sub-regions (East Asia, South Asia, and Southeast Asia), and then performed a classical multidimensional scaling in a 2-dimensional space[65]. Finally, we summarised the trunk location within Southeastern Asia over time based on the phylogeographic estimates using PACT v.0.9.5 (https://github.com/trvrb/PACT)[26].

Sequence-based antigenic and genetic distance
As the antigenic sites have been clearly resolved for A/H3N2[28,29], we calculated sequence-based antigenic distances for A/H3N2 HA sequences[30]. In brief, in each antigenic site (A, B, C, D, and E) of A/H3N2[29], we quantify the number of differences in amino acids (Hamming distance) for aligned amino acid sequences compared to the sequence of the vaccine strain "A/Wisconsin/67/2005" (also the reference sequence in this study). Antigenic site-specific Hamming distances are divided by the total number of amino acids in the antigenic site, and then multiplied by 20, representing a 20-dimensional immunological shape space[66]. The final antigenic distance between each virus strain and "A/Wisconsin/67/2005" was calculated by averaging the above values at five antigenic sites. To identify the leading and trailing geographic regions undergoing antigenic evolution of A/H3N2, we fitted a linear best-fit line between antigenic distance against date of collection. Points to the right of the line are thought to be antigenically advanced, whereas strains to the left of the line are antigenically lagging[4]. We then summarised the leading and trailing pattern by regions and time periods. Bootstrap resampling of distance values yielded a p-value for the difference between interpandemic seasons and each pandemic season.

Considering the less resolved antigenic mapping for B/Victoria, we instead used genetic distance to capture its leading and trailing pattern. Genetic distance was estimated using the Kimura two-parameter model (K80) to account for hidden substitutions[67]. We adopted the nucleotide sites in the HA1 region of the HA segment to estimate genetic distance, in line with the antigenic distance. The consistency between antigenic distance and genetic distance for the estimates of leading and trailing patterns for A/H3N2 subtype was compared to examine the validity of this approach.

Reporting summary
Further information on research design is available in the Nature Portfolio Reporting Summary linked to this article.

Data availability
Influenza virological surveillance data were available from FluNet (https://www.who.int/tools/flunet). Genetic sequences used were downloaded from NCBI and GISAID. The origin-destination air flight data were provided by Official Airline Guide (OAG) Ltd. (https://www.oag.com/) through a data sharing agreement. Data generated in this study have been deposited in GitHub (https://github.com/zycfd/sea_flu, https://doi.org/10.5281/zenodo.14279589).

Code availability
The codes and accession IDs of sequences used to run the analyses are available here: https://github.com/zycfd/sea_flu.

References
1. Iuliano, A. D. et al. Estimates of global seasonal influenza-associated respiratory mortality: a modelling study. *Lancet* **391**, 1285–1300 (2018).
2. Brockmann, D. & Helbing, D. The hidden geometry of complex, network-driven contagion phenomena. *Science* **342**, 1337–1342 (2013).
3. Han, A. X., de Jong, S. P. J. & Russell, C. A. Co-evolution of immunity and seasonal influenza viruses. *Nat. Rev. Microbiol.* **21**, 805–817 (2023).

4. Russell, C. A. et al. The global circulation of seasonal influenza A (H3N2) viruses. *Science* **320**, 340–346 (2008).

5. Kakoullis, L. et al. Influenza: seasonality and travel-related considerations. *J. Travel Med.* **30**, taad102 (2023).

6. Perofsky, A. C. et al. Antigenic drift and subtype interference shape A(H3N2) epidemic dynamics in the United States. *eLife*. https://doi.org/10.1101/2023.10.02.23296453 (2023).

7. Gatti, L. et al. Cross-reactive immunity potentially drives global oscillation and opposed alternation patterns of seasonal influenza A viruses. *Sci. Rep.* **12**, 8883 (2022).

8. Dhanasekaran, V. et al. Human seasonal influenza under COVID-19 and the potential consequences of influenza lineage elimination. *Nat. Commun.* **13**, 1721 (2022).

9. Perofsky, A. C. et al. Impacts of human mobility on the citywide transmission dynamics of 18 respiratory viruses in pre- and post-COVID-19 pandemic years. *Nat. Commun.* **15**, 4164 (2024).

10. Chen, Z. et al. COVID-19 pandemic interventions reshaped the global dispersal of seasonal influenza viruses. *Science* **386**, eadq3003 (2024).

11. Piret, J. & Boivin, G. Viral Interference between Respiratory Viruses. *Emerg. Infect. Dis.* **28**, 273–281 (2022).

12. Pinky, L. & Dobrovolny, H. M. Epidemiological consequences of viral interference: a mathematical modeling study of two interacting viruses. *Front. Microbiol.* **13**, 830423 (2022).

13. Petrova, V. N. & Russell, C. A. The evolution of seasonal influenza viruses. *Nat. Rev. Microbiol.* **16**, 47–60 (2018).

14. Wen, F., Bedford, T. & Cobey, S. Explaining the geographical origins of seasonal influenza A (H3N2). *Proc. Biol. Sci.* **283**. https://doi.org/10.1098/rspb.2016.1312 (2016).

15. Caini, S., Schellevis, F., El-Guerche Séblain, C. & Paget, J. Important changes in the timing of influenza epidemics in the WHO European Region over the past 20 years: virological surveillance 1996 to 2016. *Euro Surveill.* **23**. https://doi.org/10.2807/1560-7917.Es.2018.23.1.17-00302 (2018).

16. Chen, C. et al. The global region-specific epidemiologic characteristics of influenza: World Health Organization FluNet data from 1996 to 2021. *Int. J. Infect. Dis.* **129**, 118–124 (2023).

17. Saha, S. et al. Influenza seasonality and vaccination timing in tropical and subtropical areas of southern and south-eastern Asia. *Bull. World Health Organ.* **92**, 318–330 (2014).

18. Cowling, B. J. et al. Influenza in the Asia-Pacific region: Findings and recommendations from the Global Influenza Initiative. *Vaccine* **35**, 856–864 (2017).

19. Smith, G. J. et al. Origins and evolutionary genomics of the 2009 swine-origin H1N1 influenza A epidemic. *Nature* **459**, 1122–1125 (2009).

20. Paget, J., Caini, S., Del Riccio, M., van Waarden, W. & Meijer, A. Has influenza B/Yamagata become extinct and what implications might this have for quadrivalent influenza vaccines? *Eur. Surveill.* **27**, 2200753 (2022).

21. World Health Organization. *Review of Global Influenza Circulation, Late 2019 to 2020, and the Impact of the COVID-19 Pandemic on Influenza Circulation*. https://www.who.int/publications/i/item/who-wer-9625-241-264 (WHO, 2021).

22. SteelFisher, G. K. et al. Public response to the 2009 influenza A H1N1 pandemic: a polling study in five countries. *Lancet Infect. Dis.* **12**, 845–850 (2012).

23. Chen, Y. et al. Global pattern and determinant for interaction of seasonal influenza viruses. *J. Infect. Public Health* **17**, 1086–1094 (2024).

24. GBD 2015 DALYs and HALE Collaborators. Global, regional, and national disability-adjusted life-years (DALYs) for 315 diseases and injuries and healthy life expectancy (HALE), 1990-2015: a systematic analysis for the Global Burden of Disease Study 2015. *Lancet* **388**, 1603–1658 (2016).

25. Layan, M. et al. Impact and mitigation of sampling bias to determine viral spread: evaluating discrete phylogeography through CTMC modeling and structured coalescent model approximations. *Virus Evol.* **9**, vead010 (2023).

26. Bedford, T. et al. Global circulation patterns of seasonal influenza viruses vary with antigenic drift. *Nature* **523**, 217–220 (2015).

27. Rambaut, A. et al. The genomic and epidemiological dynamics of human influenza A virus. *Nature* **453**, 615–619 (2008).

28. Wiley, D. C., Wilson, I. A. & Skehel, J. J. Structural identification of the antibody-binding sites of Hong Kong influenza haemagglutinin and their involvement in antigenic variation. *Nature* **289**, 373–378 (1981).

29. Skowronski, D. M. et al. Low 2012-13 influenza vaccine effectiveness associated with mutation in the egg-adapted H3N2 vaccine strain not antigenic drift in circulating viruses. *PloS ONE* **9**, e92153 (2014).

30. Anderson, C. S., McCall, P. R., Stern, H. A., Yang, H. & Topham, D. J. Antigenic cartography of H1N1 influenza viruses using sequence-based antigenic distance calculation. *BMC Bioinform.* **19**, 51 (2018).

31. Bedford, T. et al. Integrating influenza antigenic dynamics with molecular evolution. *eLife* **3**, e01914 (2014).

32. Matteson, N. L. et al. Genomic surveillance reveals dynamic shifts in the connectivity of COVID-19 epidemics. *Cell*. https://doi.org/10.1016/j.cell.2023.11.024 (2023).

33. Adams, B. & McHardy, A. C. The impact of seasonal and year-round transmission regimes on the evolution of influenza A virus. *Proc. R. Soc. B Biol. Sci.* **278**, 2249–2256 (2010).

34. Kistler, K. E. & Bedford, T. An atlas of continuous adaptive evolution in endemic human viruses. *Cell Host Microbe* **31**, 1898–1909.e1893 (2023).

35. Vijaykrishna, D. et al. The contrasting phylodynamics of human influenza B viruses. *eLife* **4**, e05055 (2015).

36. Qiu, Z. et al. The effectiveness of governmental nonpharmaceutical interventions against COVID-19 at controlling seasonal influenza transmission: an ecological study. *BMC Infect. Dis.* **22**, 331 (2022).

37. Caini, S. et al. Probable extinction of influenza B/Yamagata and its public health implications: a systematic literature review and assessment of global surveillance databases. *Lancet Microbe* **5**, 100851 (2024).

38. Goldstein, E., Cobey, S., Takahashi, S., Miller, J. C. & Lipsitch, M. Predicting the epidemic sizes of influenza A/H1N1, A/H3N2, and B: a statistical method. *PLoS Med.* **8**, e1001051 (2011).

39. Cauchemez, S. et al. School closures during the 2009 influenza pandemic: national and local experiences. *BMC Infect. Dis.* **14**, 207 (2014).

40. Hay, J. A. et al. Reconstructed influenza A/H3N2 infection histories reveal variation in incidence and antibody dynamics over the life course. *PLoS Biol.* **22**, e3002864 (2024).

41. World Health Organization. *Global Influenza Surveillance and Response System (GISRS)*. https://www.who.int/initiatives/global-influenza-surveillance-and-response-system (WHO, 2024).

42. Park, S. W., Cobey, S., Metcalf, C. J. E., Levine, J. M. & Grenfell, B. T. Predicting pathogen mutual invasibility and co-circulation. *Science* **386**, 175–179 (2024).

43. World Health Organization. *Global Epidemiological Surveillance Standards for Influenza*. https://iris.who.int/handle/10665/311268 (WHO, 2013).

44. Hale, T. et al. A global panel database of pandemic policies (Oxford COVID-19 Government Response Tracker). *Nat. Hum. Behav.* **5**, 529–538 (2021).

45. Genuer, R., Poggi, J.-M. & Tuleau-Malot, C. VSURF: an R package for variable selection using random forests. *R. J.* **7**, 19–33 (2015).

46. Bonacina, F. et al. Global patterns and drivers of influenza decline during the COVID-19 pandemic. *Int. J. Infect. Dis.* **128**, 132–139 (2023).

47. United Nations, Department of Economic and Social Affairs, Population Division. *2024 Revision of World Population Prospects*. (United Nations, 2024).

48. Hadfield, J. et al. Nextstrain: real-time tracking of pathogen evolution. *Bioinformatics* **34**, 4121–4123 (2018).

49. Ivan, A., Cornelius, R., Emma, B. H. & Richard, A. N. Nextclade: clade assignment, mutation calling and quality control for viral genomes. *J. Open Source Softw.* **6**, 3773 (2021).

50. Yu, H. et al. Characterization of regional influenza seasonality patterns in China and implications for vaccination strategies: spatio-temporal modeling of surveillance data. *PLoS Med.* **10**, e1001552 (2013).

51. Liao, Y. et al. Characterization of influenza seasonality in China, 2010-2018: Implications for seasonal influenza vaccination timing. *Influenza Other Respir. Viruses* **16**, 1161–1171 (2022).

52. Lemey, P. et al. Unifying viral genetics and human transportation data to predict the global transmission dynamics of human influenza H3N2. *PLoS Pathog.* **10**, e1003932 (2014).

53. Yang, B. et al. Comparison of control and transmission of COVID-19 across epidemic waves in Hong Kong: an observational study. *Lancet Reg. Health West. Pac.* **43**, 100969 (2024).

54. World Health Organization. *Vaccines in Tropics and Subtropics*. https://www.who.int/teams/global-influenza-programme/vaccines/vaccine-in-tropics-and-subtropics (WHO, 2024).

55. Minh, B. Q. et al. IQ-TREE 2: new models and efficient methods for phylogenetic inference in the genomic era. *Mol. Biol. Evol.* **37**, 1530–1534 (2020).

56. Rambaut, A., Lam, T. T., Max Carvalho, L. & Pybus, O. G. Exploring the temporal structure of heterochronous sequences using TempEst (formerly Path-O-Gen). *Virus Evol.* **2**, vew007 (2016).

57. Sagulenko, P., Puller, V. & Neher, R. A. TreeTime: maximum-likelihood phylodynamic analysis. *Virus Evol.* **4**, vex042 (2018).

58. Suchard, M. A. et al. Bayesian phylogenetic and phylodynamic data integration using BEAST 1.10. *Virus Evol.* **4**, vey016 (2018).

59. Ayres, D. L. et al. BEAGLE 3: improved performance, scaling, and usability for a high-performance computing library for statistical phylogenetics. *Syst. Biol.* **68**, 1052–1061 (2019).

60. Minin, V. N. & Suchard, M. A. Fast, accurate and simulation-free stochastic mapping. *Philos. Trans. R. Soc. Lond. Ser. B Biol. Sci.* **363**, 3985–3995 (2008).

61. du Plessis, L. et al. Establishment and lineage dynamics of the SARS-CoV-2 epidemic in the UK. *Science* **371**, 708–712 (2021).

62. Shapiro, B., Rambaut, A. & Drummond, A. J. Choosing appropriate substitution models for the phylogenetic analysis of protein-coding sequences. *Mol. Biol. Evol.* **23**, 7–9 (2006).

63. Gill, M. S. et al. Improving Bayesian population dynamics inference: a coalescent-based model for multiple loci. *Mol. Biol. Evol.* **30**, 713–724 (2013).

64. Lemey, P. et al. Untangling introductions and persistence in COVID-19 resurgence in Europe. *Nature* **595**, 713–717 (2021).

65. Mardia, K. V. Some properties of clasical multi-dimesional scaling. *Commun. Stat. Theory Methods* **7**, 1233–1241 (1978).

66. Smith, D. J. *The Cross-Reactive Immune Response: Analysis, Modeling, and Application to Vaccine Design*. Doctor of Philosophy Thesis, The University of New Mexico. (1997).

67. Kimura, M. A simple method for estimating evolutionary rates of base substitutions through comparative studies of nucleotide sequences. *J. Mol. Evol.* **16**, 111–120 (1980).

Acknowledgements

Author contributions

H.Y. conceived and planned the research. Z.C. and P.L. analysed the data. J.L.-H.T., J.C., S. S., C.V., L.D.P., P.L., M.U.G.K. and H.Y. advised on methodologies. Z.C. wrote the initial manuscript draft. Z.C., C.V., L.D.P., P.L., M.U.G.K. and H.Y. interpreted the results and revised the content critically. All authors edited, read, and approved the manuscript.

Competing interests

Additional information

Supplementary information The online version contains supplementary material available at https://doi.org/10.1038/s41467-025-55840-y.

Correspondence and requests for materials should be addressed to Philippe Lemey, Moritz U. G. Kraemer or Hongjie Yu.

Peer review information *Nature Communications* thanks Justin Bahl and the other, anonymous, reviewer(s) for their contribution to the peer review of this work. A peer review file is available.

Reprints and permissions information is available at http://www.nature.com/reprints